https://dx.doi.org/10.1016/j.cej.2023.145295

Manipulating the Excited States from Charge-Transfer to Hybridized Local and Charge-Transfer towards High-Performance Blue Electroluminescence

He Jiang,[a,b#] Hanlin Li,[c#] Jiahao Qiu,[d] Jibiao Jin,[a,b] Chunying Xi,[d] Peng Tao,*[a,b] Baohua Zhang,*[d] Dongge Ma,*[c] and Wai-Yeung Wong*[a,b]

[a]Department of Applied Biology and Chemical Technology and Research Institute for Smart Energy, The Hong Kong Polytechnic University, Hung Hom, Hong Kong, P. R. China

[b]The Hong Kong Polytechnic University Shenzhen Research Institute, Shenzhen 518057, P. R. China

[c]State Key Laboratory of Luminescent Materials and Devices, Center for Aggregation-Induced Emission, South China University of Technology, Guangzhou 510640, P. R. China

[d]Center for Advanced Analytical Science, Guangzhou Key Laboratory of Sensing Materials and Devices, Guangdong Engineering Technology Research Center for Photoelectric Sensing Materials and Devices, c/o School of Chemistry and Chemical Engineering, Guangzhou University, Guangzhou 510006, P. R. China.

Email: pengtao@polyu.edu.hk (P. Tao); ccbhzhang@gzhu.edu.cn (B. Zhang); msdgma@scut.edu.cn (D. Ma); wai-yeung.wong@polyu.edu.hk (W.-Y. Wong)

ABSTRACT: Manipulating the excited states of organic luminescent materials can efficiently improve the utilization of both singlet and triplet excitons for developing high-performance organic light-emitting diodes (OLEDs), but the issue remains difficult due to the lack of well-controlled ways. Here, we proposed a molecular design strategy of excited state manipulation from charge-transfer (CT) to hybridized local and charge-transfer (HLCT) via adjusting the cyano position on pyridine acceptor. The *meta*-substituted **PyAn4CN** is mainly composed of a CT component, while the *para*-substituted **PyAn5CN** is endowed with a HLCT component. On further extending the conjugation of **PyAn5CN** by inserting a benzene unit between the pyrene and anthracene core, the HLCT character is preserved in **PyPhAn5CN**, accompanied by a faster radiative decay. Consequently, the vacuum-evaporated OLEDs exhibit blue

electroluminescence (EL) with the emission peaks in the range of 455-460 nm and high external quantum efficiency (EQE) up to 7.52%, together with well-suppressed efficiency roll-offs of 0.8% and 3.7% at the luminance of 100 and 1000 cd m^{-2}, respectively. More importantly, the solution-processed device shows an excellent performance with EQE of 6.49%, which is one of the best results in the solution-processed HLCT OLEDs. Our results clearly indicate that the formation of HLCT state is an efficient way to realize high-efficiency blue electrofluorescence.

Keywords: organic light-emitting diode, hybridized local and charge-transfer, charge-transfer, excited state, electroluminescence

1. Introduction

As the essential component, organic fluorescent emitters play a key role to determine the performance of organic light-emitting diodes (OLEDs).[1-6] The conventional fluorescent emitters can only utilize singlet excitons for light emission while the triplet excitons are lost through non-radiative processes, thus limiting the internal quantum efficiency (IQE) of 25% because of the ratio of the formed singlet and triplet excitons of 1:3 according to the spin statistics under electrical excitation.[7-11] Therefore, how to make an effective utilization of triplet exciton is a crucial issue to obtain high-efficiency electroluminescence (EL). Recently, triplet-triplet annihilation (TTA) emitters capable of converting two triplet excitons to generate one singlet exciton for emission have an enhanced IQE of 62.5%, breaking the theoretical IQE limit of 25% and achieving the external quantum efficiency (EQE) over 10%.[12-17] In thermally activated delayed fluorescence (TADF) emitters, 75% triplet excitons can be made with a full utilization to realize an ideal 100% IQE through reverse intersystem crossing (RISC) process, up to now, the reported EQEs of TADF devices are over 40%.[3, 18-20] But most of the TADF emitters are constructed by donor-acceptor (D-A) structure to give a small singlet-triplet energy gap (ΔE_{ST}) for efficient RISC process, such D-A structure usually makes the molecules to possess a strong charge-transfer (CT) character, accompanied by a broad and red-shifted emission.[21-23] In addition, the TADF devices always suffer from severe efficiency roll-off due to the long-lived triplet excitons.[24]

Therefore, there is a great challenge to design blue TADF emitters for high-performance blue EL devices.

Recently, a new kind of fluorescent emitters, hybridized local and charge-transfer (HLCT)-type materials with a high-lying excited state formed by a highly mixed or hybridized locally excited (LE) and CT state, has been developed by Ma and co-workers.[25-27] Different from TADF feature, the RISC process in HLCT emitters occurs at the high-lying excited states via a "hot exciton" channel, named hRISC process, thus realizing IQE of 100%.[26, 28] Generally, the LE state in the HLCT emitters gives a large transition moment to a highly efficient fluorescent radiative decay, while the CT state ensures the generation of a high fraction of singlet exciton for full exciton utilization.[29-32] Because the development of HLCT emitters is still in its infancy, the efficiency is inferior than TADF emitters, and more efforts need to be made for the advance of this research area. With respect to the design of HLCT emitters, the rational manipulation of the excited states is crucial to achieve high-efficiency EL devices.

Herein, we proposed an effective molecular design strategy by introducing a N-containing cyanopyridine acceptor to construct a series of blue fluorescent emitters (Fig. 1). Owing to the enhanced electron-withdrawing ability than that of the benzonitrile moiety, the prepared molecules with the increased CT components show red-shifted emissions in the range of 455-468 nm compared with the benzonitrile derivative (437 nm) (Supporting Information). By changing the cyano group from *meta* to *para* position, torsional angle between anthracene and cyanopyridine acceptor at the lowest singlet excited state (S_1) is obviously decreased due to the reduced steric hindrance (Fig. S1), attributing to the excited state manipulation from CT to HLCT state, thus leading to an increased photoluminescence quantum yield (PLQY) of 73%. By further inserting a phenyl ring between pyrene and anthracene core, the intermolecular electronic couplings can be enhanced and the charge transport properties can be optimized in **PyPhAn5CN**, while its emission remains unchanged due to the same transition component of S_1 state (Fig. 2a). The vacuum-evaporated OLEDs based on these emitters exhibited blue EL emission with high EQEs up to 7.52%. More importantly,

the solution-processed device showed an excellent performance with high maximum EQE of 6.49% and current efficiency (CE) of 10.54 cd A^{-1}, which are one of the highest values in the solution-processed HLCT OLEDs. [33-38]

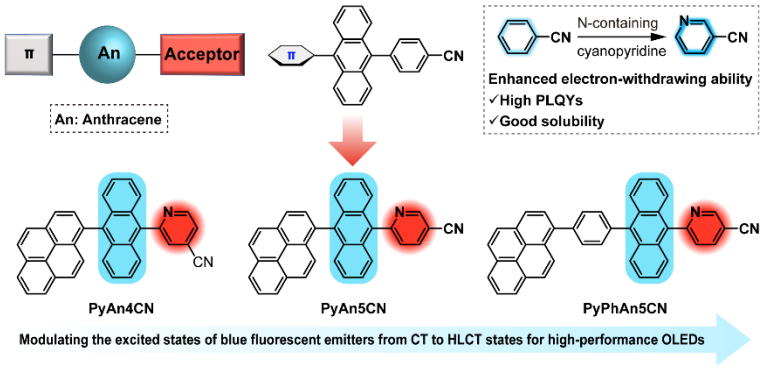

Fig. 1. Molecular design strategy and chemical structures of blue anthracene-based fluorescent emitters.

2. Results and Discussion

2.1 Molecular Design and Simulation

As illustrated in Fig. 1, cyanopyridine, anthracene and pyrene units were chosen as the electron-acceptor, electron-donor and peripheral π-conjugation moiety to construct three blue fluorescent emitters **PyAn4CN PyAn5CN** and **PyPhAn5CN**. These emitters show similar lowest unoccupied molecular orbital (LUMO) distributions, which are localized on the anthracene core and the cyanopyridine acceptor (Fig. 2a). The highest occupied molecular orbitals (HOMOs) of **PyAn4CN** and **PyAn5CN** are distributed on the anthracene moiety, while that of **PyPhAn5CN** is localized on both anthracene and pyrene units, suggesting that the good charge-transporting properties can be realized in **PyPhAn5CN** due to the electron-donating ability of the peripheral pyrene moiety and a reduced torsion angle between pyrene and anthracene groups induced by a phenyl linker (Fig. 2a).[39] In order to investigate their excited-state characteristics, natural transition orbital (NTO) analysis was performed (Fig. 2a and Fig. S2). For the $S_0 \rightarrow S_1$ transition of *meta*-substituted **PyAn4CN**, the "hole" and "particle" are separated from each other, indicating a CT-dominant excited state with a small oscillator strength (*f*) of 0.0398. Differently, the "hole" of *para*-substituted **PyAn5CN** and **PyPhAn5CN** is distributed on the anthracene core, and the "particle"

is localized on the anthracene and cyanopyridine acceptor, which shows the obvious HLCT states with the enhanced *f* values of 0.2132 and 0.2359. Furthermore, the large energy gap (~1.20 eV) between T_1 and T_3 or T_4 suppressed the internal conversion (IC) process and the small energy gap (~0.03 eV) between S_1 and T_3 or T_4 promoted the hRISC process (Fig. 2b).[26] Meanwhile, their energy gaps (0.65-0.82 eV) between S_1 and T_2 states were larger than those between T_1 and T_2 states (~0.3 eV), thus leading to the fast IC process instead of hRISC from T_2 to T_1 state. It should be noticed that they exhibit relatively high spin-orbit coupling (SOC) constants (~0.5 cm^{-1}) between S_1 and T_3 or T_4. Thus with the help of small energy gap and large SOC constant, the hRISC processes between S_1 and T_3 or T_4 in **PyAn5CN** and **PyPhAn5CN** will be very efficient to make full utilization of the triplet excitons.[40]

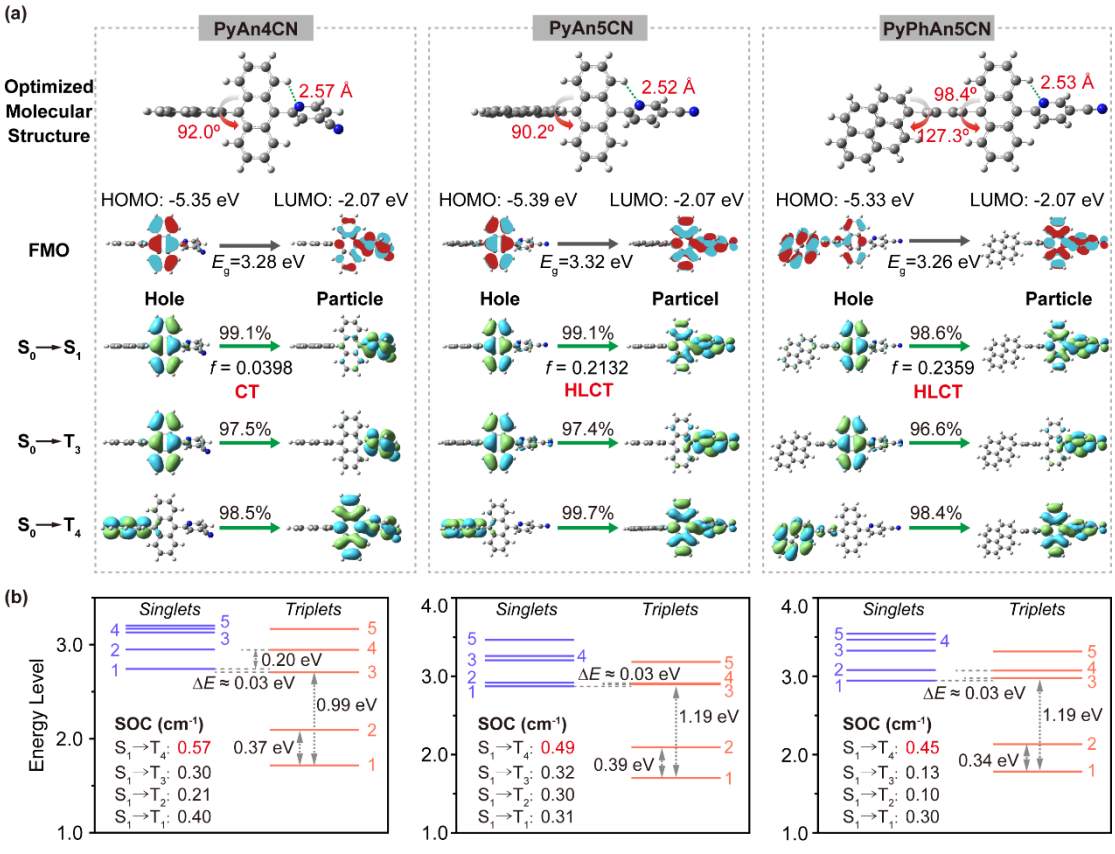

Fig. 2. (a) Optimized geometric structures, HOMO and LUMO distributions, NTO analysis and (b) energy level diagrams including SOC constants of **PyAn4CN**, **PyAn5CN** and **PyPhAn5CN**.

2.2 Synthesis and Characterization

The synthetic routes of the newly prepared emitters were shown in Scheme S1 and S2 in the Supporting Information. The intermediate arylboronic acids were synthesized via lithiation-borylation reaction and another kind of Br-substituted anthracene intermediates was obtained in two identical steps through Suzuki cross-couplings followed by bromination of anthracene segment. The synthesis of **PyAn4CN**, **PyAn5CN** and **PyPhAn5CN** were finally achieved by Suzuki cross-couplings between the corresponding arylboronic acid and bromoanthracene intermediate in high yields. Their molecular structures were fully characterized by ^{1}H NMR and ^{13}C NMR spectroscopy, mass spectrometry (Supporting Information) and single crystal analysis (Fig. S3 and Table S1). It should be noted that the torsion angle between pyrene and anthracene groups was 84.24º in **PyAn4CN** (Fig. S3), indicating its highly twisted molecular configuration. The thermal properties of these three emitters were investigated via thermogravimetric analysis (TGA) and differential scanning calorimetry (DSC) measurements (Fig. S4). The decomposition temperatures (T_d: 5% weight loss) for **PyAn4CN**, **PyAn5CN** and **PyPhAn5CN** were 389, 399 and 418 ℃, respectively, and the melting temperatures (T_m) in DSC curves were 290 ℃ for **PyAn4CN** and 318 ℃ for **PyPhAn5CN**, but there was no T_m or glass-transition temperature (T_g) observed for **PyAn5CN**, probably due to its narrow T_m or T_g range.[41] These high thermal stabilities were beneficial for the practical applications in EL devices.[42]

2.3 Photophysical Properties

The UV-vis absorption and photoluminescence (PL) spectra were measured to study the photophysical properties of **PyAn4CN**, **PyAn5CN** and **PyPhAn5CN** (Fig. 3a and 3b). The lower-energy absorption bands within 350−400 nm belong to the vibrational characteristics from π-π* transitions of the central anthracene unit, while the higher-energy absorption bands at around 290−350 nm were assigned to π-π* transition from the pyrene moiety (Fig. 3a and Fig. S5).[13, 39, 43] These emitters in dilute toluene exhibited similar blue emissions at 455−468 nm to the molecule of An5CN without a pyrene unit (Fig. S6), and the PL emission peaks were at 473−479 nm in films , showing

spectral red-shifts of 18, 11, 11 nm for **PyAn4CN**, **PyAn5CN** and **PyPhAn5CN**, respectively (Fig. 3b and Table 1). The PLQYs of **PyAn4CN**, **PyAn5CN** and **PyPhAn5CN** in toluene were measured to be 61%, 73% and 65%, while those in the doped films were 41%, 36% and 69%, respectively. The enhanced PLQYs of **PyAn5CN** and **PyPhAn5CN** were benefited from the increased LE components and were consistent with their larger oscillator strength (Fig. 2a). Then, their fluorescent behaviors were investigated by transient PL analysis. As shown in Fig. 3c, all the emitters exhibited short nanosecond-scaled excited lifetimes of 4.19, 4.10 and 1.67 ns for **PyAn4CN**, **PyAn5CN** and **PyPhAn5CN**, respectively, and did not show delayed fluorescence component. It should be noted that the shortest excited state lifetime of **PyPhAn5CN** is probably due to the increased non-radiative decay population caused by the molecular motion attributed to the bridged phenyl unit.[44] The corresponding non-radiative decay rates were calculated to be 1.0×10^{8} s^{-1} for **PyAn4CN**, 6.0×10^{7} s^{-1} for **PyAn5CN**, and 2.1×10^{8} s^{-1} for **PyPhAn5CN**, respectively. Moreover, the solvatochromic effects of three emitters were analyzed in different solvents from low-polarity cyclohexane to high-polarity acetonitrile (Fig. 3d). It was found that the emission peaks of three emitters were gradually red-shifted with increasing the polarity of solvent, and the reduced red-shifts from 24 nm to 14 nm was profited from the enhanced LE components of HLCT excited states (Fig. S7).[31, 45] Further analysis from the Lippert-Mataga models (Fig. S8 and Table S2), **PyAn4CN** exhibited a linear relationship between the Stokes shift and the orientation polarizability of solvent, while that of **PyAn5CN** and **PyPhAn5CN** was demonstrated as two different linear plots, indicating that their excited states with HLCT character.[30]

To better determinate the excited states, the low temperature fluorescence and phosphorescence spectra of three emitters at 77 K were investigated (Fig. S9). According to the formula $E_{S_1} = 1240/\lambda_{PL}$, the S_1 value of these three emitters were calculated to be 2.69, 2.62 and 2.63 eV for **PyAn4CN** and **PyAn5CN** and **PyPhAn5CN**, respectively. By using a phosphorescent dye PtOEP to sensitize the T_1 states of the prepared emitters, the new emission peaks at around 700 nm were reasonably assigned to the T_1 states of three blue emitters, while the peaks located at 430-560 nm were attributed to their high-lying triplet excited state T_n (n = 2, 3 or 4), thus the corresponding T_1, T_2, T_3 and T_4 values were 1.78, 2.22, 2.49 and 2.84 eV for **PyAn4CN**, 1.77, 2.16, 2.42 and 2.79 eV for **PyAn5CN**, and 1.73, 2.21, 2.53 and 2.74 eV **PyPhAn5CN**, respectively (Fig. S9). These results clearly demonstrated the existence of much lower T_1 energy levels of ≈1.77 eV and large energy gaps of ≈0.90 eV between

S_1 and T_1, promoting the hRISC process to occur.[46]

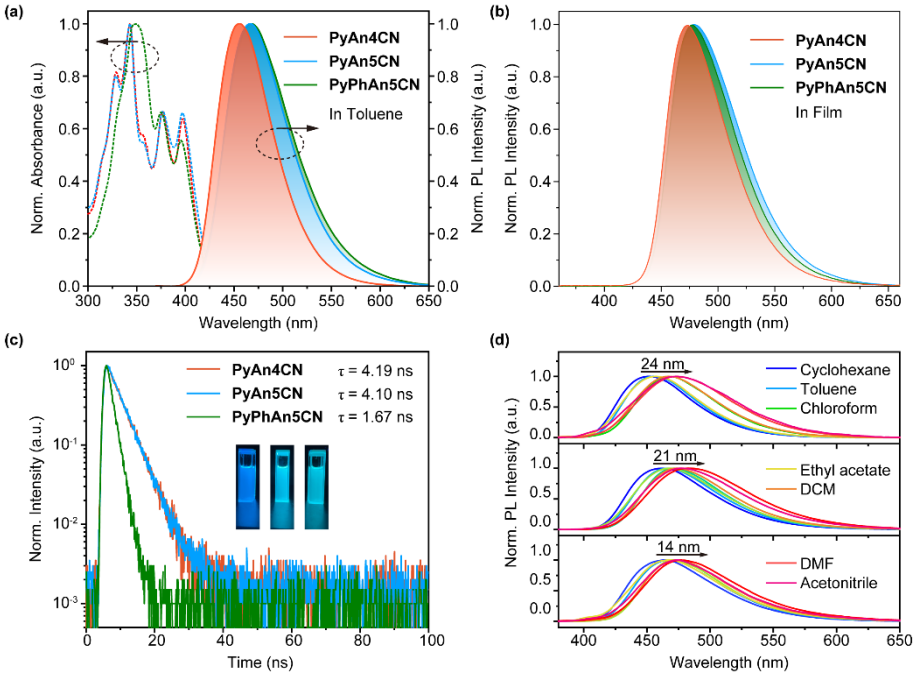

Fig. 3. (a) UV-vis absorption spectra and PL spectra (10^{-5} M in toluene), (b) PL spectra in films, (c) transient PL decay curves (10^{-5} M in toluene), and (d) solvatochromic effect spectra of **PyAn4CN**, **PyAn5CN** and **PyPhAn5CN**. Inset are their PL photographs in toluene under UV light.

Table 1. The thermal, photophysical and electrochemical properties of **PyAn4CN**-, **PyAn5CN**- and **PyPhAn5CN**-based devices.

Compound	T_d/T_m[a] (°C)	λ_{abs}[b] (nm)	λ_{em}[b] (nm)	λ_{em}[c] (nm)	E_g[d] (eV)	E_{S_1}[e] (eV)	HOMO/LUMO[f] (eV)	PLQY[g] (%)
PyAn4CN	389/290	328, 342, 375, 396	455	473	2.95	2.73/2.62	-5.82/-2.87	61/17/41
PyAn5CN	399/-	327, 341, 375, 396	467	478	2.92	2.66/2.59	-5.82/-2.90	73/13/36
PyPhAn5CN	418/318	348, 374, 394	468	479	2.94	2.65/2.59	-5.77/-2.83	65/40/69

[a] Decomposition temperature (5% weight loss)/melting point; [b] Measured in toluene; [c] Measured in neat film; [d] Calculated from absorption onset in toluene; [e] Calculated from emission peak in toluene and film at room temperature; [f] HOMO: estimated by cyclic voltammetry measurement; LUMO: calculated from the equation: $E_{LUMO} = E_{HOMO} + E_g$; [g] Absolute PLQY evaluated by integrating sphere in toluene, neat and doped films.

2.4 Electrochemical Properties

The electrochemical properties of **PyAn4CN**, **PyAn5CN** and **PyPhAn5CN** were studied by electrochemical cyclic voltammetry (CV) measurements (Fig. S10). From the onset oxidation potentials of the CV curves, the HOMO energy levels of **PyAn4CN**,

PyAn5CN and **PyPhAn5CN** were obtained as -5.82, -5.82 and -5.77 eV, respectively. Based on the equation $E_{LUMO} = E_{HOMO} + E_g$, where E_g is the optical gap from the absorption spectra, their LUMO energy levels were calculated to be -2.87, -2.90 and -2.83 eV, respectively. Their suitable HOMO and LUMO energy levels were beneficial for good charge injection in EL devices.

2.5 Device Performance

Encouraged by the appealing PL properties and good thermal stabilities of **PyAn4CN**, **PyAn5CN** and **PyPhAn5CN**, the vacuum-evaporated OLED devices with a configuration of ITO/HATCN (15 nm)/TAPC (50 nm)/TCTA (5 nm)/CZPA: 5 wt% emitter (20 nm)/TmPyPB (40 nm)/LiF (1 nm)/Al (100 nm) were fabricated (**PyAn4CN**, **PyAn5CN** and **PyPhAn5CN** for devices A−C, respectively), in which HATCN (dipyrazino(2,3-f:20,30-h)quinoxaline-2,3,6,7,10,11-hexacarbonitrile), TAPC (4,4′-cyclohexylidenebis(*N*,*N*-bis(4-methylphenyl)benzenamine)), TCTA (4,4′,4″tris(*N*-carbazolyl)triphenylamine), TmPyPB (1,3,5-tri[(3-pyridyl)-phen-3-yl]benzene), CZPA (9-[4-(10-phenyl-9-anthryl)phenyl]-9*H*-carbazole) serve as the hole injection layer, the hole transporting layer, the electron transporting and the exciton-blocking layers, and the host, respectively. The corresponding energy level diagrams and molecular structures of the materials involved in the OLEDs are displayed in Fig. 4a and Fig. S11.

As expected, all the devices exhibited blue emissions with the EL peaks of 455, 460, and 459 nm, corresponding to the Commission Internationale de l´Eclairage (CIE) coordinates of (0.15, 0.10), (0.15, 0.16), and (0.15, 0.15) for devices A−C, respectively (Fig. 4b), which were almost identical to their PL spectra of the doped films with the same doping concentration (Fig. S12). The maximum CEs, power efficiencies (PEs), and EQEs of the devices were 6.11 cd A^{-1}, 5.25 lm W^{-1}, and 6.12% for **PyAn4CN**, 7.98 cd A^{-1}, 6.96 lm W^{-1}, and 5.75% for **PyAn5CN**, and 9.99 cd A^{-1}, 8.66 lm W^{-1}, and 7.52% for **PyPhAn5CN** (Fig. 4c and 4d and Table 2), which are among the best results reported so far and much better than those of the An5CN-based device with maximum CE of 1.03 cd A^{-1}, PE of 0.32 lm W^{-1}, and EQE of 1.08% (Fig. S13), indicating that the peripheral π-conjugation moiety of pyrene units would achieve good charge transport

property for efficient EL.[39] Remarkably, it should be noted that the CEs and PEs of **PyAn5CN**- and **PyPhAn5CN**-based devices were higher than that of **PyAn4CN**-based device, while the highest EQE in **PyPhAn5CN**-based device was observed, which was benefited from the HLCT properties. In addition, **PyAn5CN**- and **PyPhAn5CN**-based devices showed significantly reduced roll-offs (1.2% and 2.6%, and 0.8% and 3.7% at the luminance of 100 and 1000 cd m^{-2}, respectively), compared to **PyAn4CN**-based device (3.4% and 7.8% at the luminance of 100 and 1000 cd m^{-2}, respectively). Such extremely low efficiency roll-offs could be attributed to the reduced triplet exciton density at high current density via hRISC process in HLCT emitters.[47] Theoretically, the exciton utilization efficiency (EUE) of device were estimated according to following equation: $\eta_{EQE} = \eta_{eh} \times \eta_{PL} \times \eta_{exciton} \times \eta_{out}$ (η_{eh} is the factor of the recombination efficiency of injected electrons and holes, ideally 100%; η_{PL} is the absolute PLQY of the emitter; $\eta_{exciton}$ and η_{out} are the EUE of device and the light out-coupling efficiency, respectively). Therefore, the EUEs of the Devices A-C were as high as 50.2%, 39.4% and 57.8%, respectively, which broke the limit of 25% in the traditional fluorescent OLED devices, implying the effectiveness of HLCT OLEDs. To gain a deep understanding of the emission mechanism of emitters, the magnetic effect measurements on devices were carried out (Fig. S14). It should be noted that the EL intensities of these devices increased with increasing the magnetic field, further confirming that the emission mechanisms of these three emitters were not attributed to the TTA process but to the “hot exciton” channel.[46]

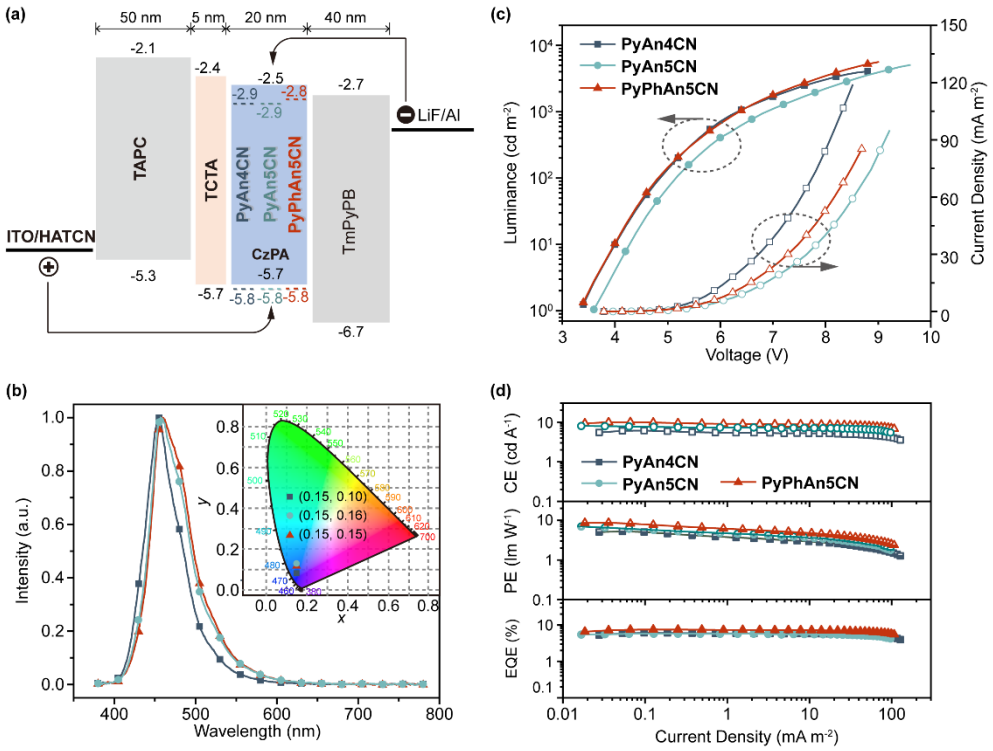

Fig. 4. EL performance of the vacuum-evaporated **PyAn4CN**-, **PyAn5CN**-, and **PyPhAn5CN**-based blue devices. (a) Device configurations and energy levels of the materials, (b) EL spectra, (c) variation of luminance (solid symbols)-voltage-current density (*J*, hollow symbols) curves, and (d) efficiencies-current density curves of the OLEDs. Inset: CIE coordinates of the vacuum-evaporated blue OLEDs based on **PyAn4CN**, **PyAn5CN**, and **PyPhAn5CN**.

Table 2. Summary of the electroluminescence performance of **PyAn4CN**-, **PyAn5CN**- and **PyPhAn5CN**-based devices.

Device	V_{on}[a] (V)	L_{max}[b] (cd m^{-2})	CE_{max}[c] (cd A^{-1})	PE_{max}[d] (lm W^{-1})	EQE[e] (%)	λ_{EL}[f] (nm)	FWHM[g] (nm)	CIE[h] (x, y)
A	3.4	4010	6.11	5.25	6.12, 5.91, 5.64	455	50	(0.15, 0.10)
B	3.6	5463	7.98	6.96	5.75, 5.68, 5.60	460	56	(0.15, 0.16)
C	3.4	6717	9.99	8.66	7.52, 7.46, 7.24	459	54	(0.15, 0.15)
D	4.0	2092	10.54	7.35	6.49, 6.01, 2.91	466	71	(0.16, 0.22)

[a] Voltage at 1 cd m^{-2}. [b] Maximum luminance. [c] Maximum current efficiency. [d] Maximum power efficiency. [e] Maximum external quantum efficiency, external quantum efficiencies at 100 and 1000 cd m^{-2}. [f] EL peak at 7 V. [g] Full width at half maximum of EL spectrum at 7 V. [h] Commission Internationale de l'E´clairage coordinate at 7 V.

In light of the good solubility and morphological stability (Fig. S15) of **PyAn5CN**, the solution-processed OLED was also fabricated with a device structure of

ITO/PEDOT:PSS (ca. 40 nm)/CZPA: 10 wt% emitter (ca. 40 nm)/bis[2-(diphenylphosphino)phenyl]ether oxide (DPEPO) (10 nm)/TmPyPB (50 nm)/LiF (1 nm)/Al (100 nm) as device D. Excitedly, device D exhibited a blue emission with an excellent maximum EQE of 6.49 %, high maximum CE up to 10.54 cd A^{-1}, and the CIE coordinate of (0.16, 0.22) (Fig. 5 and Table 2). Such high device performance should be attributed to the high exciton utilization of the HLCT emitter induced by the efficient hRISC process from the high-lying triplet excited state to the S_1 state.[25] It should be noted that these efficiencies are one of the best performances in the reported solution-processed blue HLCT OLEDs (Table S3 and Fig. S16).

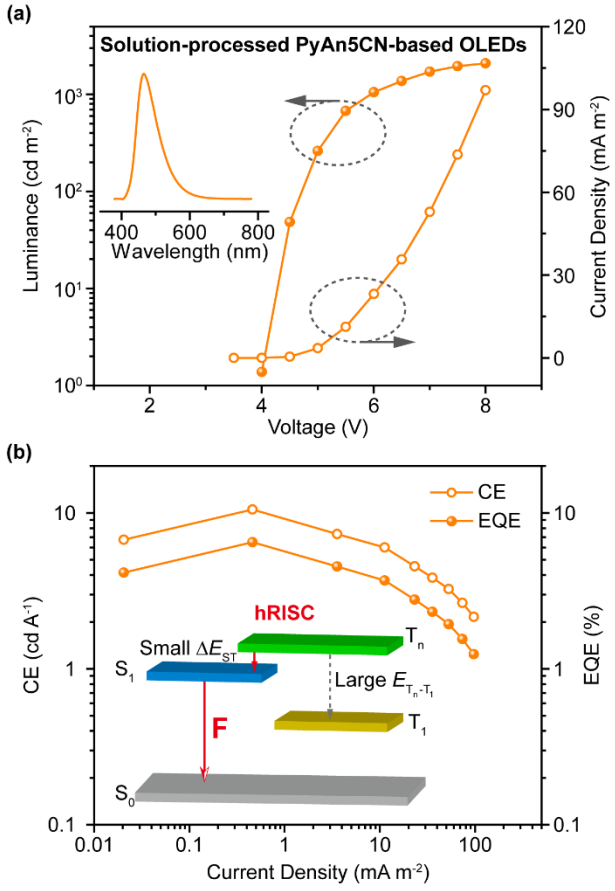

Fig. 5. (a) Luminance (solid symbols)-voltage-current density (*J*, hollow symbols) curves of the solution-processed **PyAn5CN**-based blue OLED, (b) CE-current density-EQE curves of the device. Inset: EL spectra at the voltage of 7 V.

3. Conclusion

In summary, by using cyanopyridine acceptor, anthracene core, and pyrene unit as the

building blocks, three new blue fluorescent emitters (**PyAn4CN**, **PyAn5CN** and **PyPhAn5CN**) showing controllable excited states were rationally designed, prepared and fully characterized. The theoretical simulations and experimental results elucidated that their excited states can be modulated from CT to HLCT through a simple design strategy. As a result, the vacuum-evaporated blue HLCT OLEDs based on these emitters exhibited high EQEs up to 7.52% with well-suppressed efficiency roll-offs of 0.8% and 3.7% at the luminance of 100 and 1000 cd m^{-2}, owing to the efficient hRISC process from the high-lying triplet excited state to the S_1 state. In addition, because of the high PLQY and good solubility of **PyAn5CN**, its solution-processed device was also fabricated with an excellent performance with high maximum EQE of 6.49% and CE of 10.54 cd A^{-1}, which are one of the highest efficiencies in the solution-processed HLCT OLEDs reported so far. These outstanding performances demonstrate that the relational design of the efficient HLCT emitters will be an efficient way to develop low-cost and high-efficiency blue electroluminescence.

Acknowledgements

HJ and HL contributed equally to this work. We thank Prof. David Lee Phillips and Mr. Ziqi Deng for helpful discussion. We acknowledge the National Key R&D Program of China (2022YFE0104100), National Natural Science Foundation of China (61905120, 22205188), ITC Guangdong-Hong Kong Technology Cooperation Funding Scheme (TCFS) (GHP/038/19GD), CAS-Croucher Funding Scheme for Joint Laboratories (ZH4A), Start-up Fund for RAPs under the Strategic Hiring Scheme (P0035922), Natural Science Foundation of Guangdong Province (2021A1515010510), Guangzhou Science and Technology Plan Project (20210201040), the Hong Kong Research Grants Council (PolyU 15305320), the Hong Kong Polytechnic University (YXB8), Miss Clarea Au for the Endowed Professorship in Energy (847S), and Research Institute for Smart Energy (CDAQ) for financial support.

Conflicts of Interest

The authors declare no conflict of interest.

References

[1] Y. C. Liu, C. S. Li, Z. J. Ren, S. K. Yan, M. R. Bryce, All-Organic Thermally Activated Delayed Fluorescence Materials for Organic Light-Emitting Diodes, Nat. Rev. Mater. 3 (2018), 18020.

[2] G. Hong, X. Gan, C. Leonhardt, Z. Zhang, J. Seibert, J. M. Busch and S. Brase, A Brief History of OLEDs-Emitter Development and Industry Milestones, Adv. Mater. 33 (2021), 2005630.

[3] Y. X. Hu, J. S. Miao, T. Hua, Z. Y. Huang, Y. Y. Qi, Y. Zou, Y. T. Qiu, H. Xia, H. Liu, X. S. Cao, C. L. Yang, Efficient Selenium-Integrated TADF OLEDs with Reduced Roll-Off, Nat. Photonics 16 (2022), 803-810.

[4] H. Jiang, Y. Cao, Q. Yang, L. Xian, Y. Tao, R. Chen, W. Huang, Organic Resonance Materials: Molecular Design, Photophysical Properties, and Optoelectronic Applications, J. Phys. Chem. Lett. 11 (2020), 7739-7754.

[5] Z. Zhao, C. Zeng, X. Peng, Y. Liu, H. Zhao, L. Hua, S. J. Su, S. Yan, Z. Ren, Tuning Intramolecular Stacking of Rigid Heteroaromatic Compounds for High-Efficiency Deep-Blue through-Space Charge-Transfer Emission, Angew. Chem. Int. Ed. 61 (2022), e202210864.

[6] H. Zhang, G. Li, X. Guo, K. Zhang, B. Zhang, X. Guo, Y. Li, J. Fan, Z. Wang, D. Ma, B. Z. Tang, High-Performance Ultraviolet Organic Light-Emitting Diode Enabled by High-Lying Reverse Intersystem Crossing, Angew. Chem. Int. Ed. 60 (2021), 22241-22247.

[7] Y. Wang, J. H. Yun, L. Wang, J. Y. Lee, High Triplet Energy Hosts for Blue Organic Light-Emitting Diodes, Adv. Funct. Mater. 31 (2020), 2008332.

[8] J. Y. Woo, M. H. Park, S. H. Jeong, Y. H. Kim, B. Kim, T. W. Lee, T. H. Han, Advances in Solution-Processed OLEDs and Their Prospects for Use in Displays, Adv. Mater. (2022), 2207454.

[9] M. Zhu, C. Yang, Blue Fluorescent Emitters: Design Tactics and Applications in Organic Light-Emitting Diodes, Chem. Soc. Rev. 42 (2013), 4963-4976.

[10] W.-C. Chen, C.-S. Lee, Q.-X. Tong, Blue-Emitting Organic Electrofluorescence Materials: Progress and Prospective, J. Mater. Chem. C 3 (2015), 10957-10963.

[11] P. Tao, Y. Miao, H. Wang, B. Xu, Q. Zhao, High-Performance Organic Electroluminescence: Design from Organic Light-Emitting Materials to Devices, Chem. Rec. 19 (2019), 1531-1561.

[12] C. Gao, W. W. H. Wong, Z. Qin, S. C. Lo, E. B. Namdas, H. Dong, W. Hu, Application of Triplet-Triplet Annihilation Upconversion in Organic Optoelectronic Devices: Advances and Perspectives, Adv. Mater. 33 (2021), 2100704.

[13] L. Xing, Z.-L. Zhu, J. He, Z. Qiu, Z. Yang, D. Lin, W.-C. Chen, Q. Yang, S. Ji, Y. Huo, C.-S. Lee, Anthracene-Based Fluorescent Emitters toward Superior-Efficiency Nondoped TTA-OLEDs with Deep Blue Emission and Low Efficiency Roll-Off, Chem. Eng. J. 421 (2021), 127748.

[14] H. Jiang, P. Tao, W.-Y. Wong, Recent Advances in Triplet-Triplet Annihilation-Based Materials and Their Applications in Electroluminescence, ACS Mater. Lett. 5 (2023), 822-845.

[15] S. Wang, M. Qiao, Z. Ye, D. Dou, M. Chen, Y. Peng, Y. Shi, X. Yang, L. Cui, J. Li, C. Li, B. Wei, W. Y. Wong, Efficient Deep-Blue Electrofluorescence with an External Quantum Efficiency Beyond 10%, iScience 9 (2018), 532-541.

[16] H. Lim, S. J. Woo, Y. H. Ha, Y. H. Kim, J. J. Kim, Breaking the Efficiency Limit of Deep-Blue Fluorescent OLEDs Based on Anthracene Derivatives, Adv. Mater. 34 (2022), 2100161.

[17] S. E. Seo, H.-S. Choe, H. Cho, H.-i. Kim, J.-H. Kim, O. S. Kwon, Recent Advances in Materials for and Applications of Triplet-Triplet Annihilation-Based Upconversion, J. Mater. Chem. C

10 (2022), 4483-4496.
[18] Y. Chen, D. Zhang, Y. Zhang, X. Zeng, T. Huang, Z. Liu, G. Li, L. Duan, Approaching Nearly 40% External Quantum Efficiency in Organic Light Emitting Diodes Utilizing a Green Thermally Activated Delayed Fluorescence Emitter with an Extended Linear Donor-Acceptor-Donor Structure, Adv. Mater. 33 (2021), 2103293.
[19] R. Braveenth, H. Lee, J. D. Park, K. J. Yang, S. J. Hwang, K. R. Naveen, R. Lampande, J. H. Kwon, Achieving Narrow FWHM and High EQE over 38% in Blue OLEDs Using Rigid Heteroatom-Based Deep Blue Tadf Sensitized Host, Adv. Funct. Mater. 31 (2021), 2105805.
[20] P. Jiang, J. Miao, X. Cao, H. Xia, K. Pan, T. Hua, X. Lv, Z. Huang, Y. Zou, C. Yang, Quenching-Resistant Multiresonance TADF Emitter Realizes 40% External Quantum Efficiency in Narrowband Electroluminescence at High Doping Level, Adv. Mater. 34 (2021), 2106954.
[21] Y. Tao, K. Yuan, T. Chen, P. Xu, H. Li, R. Chen, C. Zheng, L. Zhang, W. Huang, Thermally Activated Delayed Fluorescence Materials Towards the Breakthrough of Organoelectronics, Adv. Mater. 26 (2014), 7931-7958.
[22] J. Jin, W. Wang, P. Xue, Q. Yang, H. Jiang, Y. Tao, C. Zheng, G. Xie, W. Huang, R. Chen, Intermolecular Locking Design of Red Thermally Activated Delayed Fluorescence Molecules for High-Performance Solution-Processed Organic Light-Emitting Diodes, J. Mater. Chem. C 9 (2021), 2291-2297.
[23] H. Wang, B. Zhao, C. Qu, C. Duan, Z. Li, P. Ma, P. Chang, C. Han, H. Xu, 2,3-Dicyanopyrazino Phenanthroline Enhanced Charge Transfer for Efficient Near-Infrared Thermally Activated Delayed Fluorescent Diodes, Chem. Eng. J. 436 (2022), 135080.
[24] C. Yin, Y. Zhang, T. Huang, Z. Liu, L. Duan, D. Zhang, Highly Efficient and Nearly Roll-Off-Free Electrofluorescent Devices Via Multiple Sensitizations, Sci. Adv. (8) 2022, eabp9203.
[25] W. Li, Y. Pan, R. Xiao, Q. Peng, S. Zhang, D. Ma, F. Li, F. Shen, Y. Wang, B. Yang, Y. Ma, Employing ~100% Excitons in OLEDs by Utilizing a Fluorescent Molecule with Hybridized Local and Charge-Transfer Excited State, Adv. Funct. Mater. 24 (2014), 1609-1614.
[26] C. W. Lin, P. B. Han, S. Xiao, F. L. Qu, J. W. Yao, X. F. Qiao, D. Z. Yang, Y. F. Dai, Q. Sun, D. H. Hu, A. J. Qin, Y. G. Ma, B. Z. Tang, D. G. Ma, Efficiency Breakthrough of Fluorescence OLEDs by the Strategic Management of “Hot Excitons” at Highly Lying Excitation Triplet Energy Levels, Adv. Funct. Mater. 31 (2021), 2106912.
[27] S. Xiao, Y. Gao, R. Wang, H. Liu, W. Li, C. Zhou, S. Xue, S.-T. Zhang, B. Yang, Y. Ma, Highly Efficient Hybridized Local and Charge-Transfer (HLCT) Deep-Blue Electroluminescence with Excellent Molecular Horizontal Orientation, Chem. Eng. J. 440 (2022), 135911.
[28] Y. Xu, P. Xu, D. Hu, Y. Ma, Recent Progress in Hot Exciton Materials for Organic Light-Emitting Diodes, Chem. Soc. Rev. 50 (2021), 1030-1069.
[29] W. Li, Y. Pan, L. Yao, H. Liu, S. Zhang, C. Wang, F. Shen, P. Lu, B. Yang, Y. Ma, A Hybridized Local and Charge-Transfer Excited State for Highly Efficient Fluorescent OLEDs: Molecular Design, Spectral Character, and Full Exciton Utilization, Adv. Opt. Mater. 2 (2014), 892-901.
[30] X. Chen, D. Ma, T. Liu, Z. Chen, Z. Yang, J. Zhao, Z. Yang, Y. Zhang, Z. Chi, Hybridized Local and Charge-Transfer Excited-State Fluorophores through the Regulation of the Donor-Acceptor Torsional Angle for Highly Efficient Organic Light-Emitting Diodes, CCS Chem. 4 (2022), 1284-1294.
[31] S.-Y. Yang, Y.-L. Zhang, F.-C. Kong, Y.-J. Yu, H.-C. Li, S.-N. Zou, A. Khan, Z.-Q. Jiang, L.-S. Liao, π-Stacked Donor-Acceptor Molecule to Realize Hybridized Local and Charge-Transfer

Excited State Emission with Multi-Stimulus Response, Chem. Eng. J. 418 (2021), 129366.
[32] Y. Liu, L. Yang, Q. Bai, W. Li, Y. Zhang, Y. Fu, F. Ye, Highly Efficient Nondoped Blue Electroluminescence Based on Hybridized Local and Charge-Transfer Emitter Bearing Pyrene-Imidazole and Pyrene, Chem. Eng. J. 420 (2021), 129939.
[33] S. Zeng, C. Xiao, J. Zhou, Q. Dong, Q. Li, J. Lim, H. Ma, J. Y. Lee, W. Zhu, Y. Wang, Deep Blue Emitter Based on Tris (triazolo)triazine Moiety with CIE_y< 0.08 for Highly Efficient Solution-Processed Organic Light-Emitting Diodes Via Molecular Strategy of "Hot Excitons", Adv. Funct. Mater. 32 (2022), 2113183.
[34] W. Wang, K. Chen, H. Wu, Y. Long, J. Zhao, L. Jiang, S. Liu, Z. Chi, J. Xu, Y. Zhang, Benzoxazole-Based Hybridized Local and Charge-Transfer Deep-Blue Emitters for Solution-Processable Organic Light-Emitting Diodes and the In fluences of Hexahydrophthalimido, ACS Appl. Mater. Interfaces 15 (2023), 13415.
[35] R. K. Konidena, K. R. J. Thomas, D. K. Dubey, S. Sahoo, J.-H. Jou, A New Molecular Design Based on Hybridized Local and Charge Transfer Fluorescence for Highly Efficient (> 6%) Deep-Blue Organic Light Emitting Diodes, Chem. Commun. 53 (2017), 11802.
[36] M. Zhao, Q. Wei, J. Zhang, W. Li, Z. Wang, S. Du, Q. Xue, G. Xie, Z. Ge, Converting Thermally Activated Delayed Fluorescence into Hybridized Local and Charge-Transfer Via an Addition Acceptor Moiety, Org. Electron. 100 (2022), 106365.
[37] T. Sudyoadsuk, S. Petdee, P. Chasing, P. Therdkatanyuphong, C. Kaiyasuan, W. Waengdongbung, S. Namuangruk, V. Promarak, A Solution-Processable Hybridized Local and Charge-Transfer (HLCT) Phenanthroimidazole as a Deep-Blue Emitter for Efficient Solution-Processed Non-Doped Electroluminescence Device, Dyes Pigm. 195 (2021), 109712.
[38] J. D. Girase, Shahnawaz, J.-H. Jou, S. Patel, S. Vaidyanathan, Solution-Processed Deep-Blue Fluorophores Based on Phenanthroimidazole Integrated with Benzimidazole with HLCT Character for Efficient Deep-Blue Organic Light Emitting Devices, Dyes Pigm. 206 (2022), 110623.
[39] C. Tang, F. Liu, Y.-J. Xia, J. Lin, L.-H. Xie, G.-Y. Zhong, Q.-L. Fan, W. Huang, Fluorene-Substituted Pyrenes-Novel Pyrene Derivatives as Emitters in Nondoped Blue OLEDs, Org. Electron. 7 (2006), 155-162.
[40] C. Fu, S. Luo, Z. Li, X. Ai, Z. Pang, C. Li, K. Chen, L. Zhou, F. Li, Y. Huang, Z. Lu, Highly Efficient Deep-Blue OLEDs Based on Hybridized Local and Charge-Transfer Emitters Bearing Pyrene as the Structural Unit, Chem. Commun. 55 (2019), 6317-6320.
[41] X. Jin, X. Xu, X. Zhang, Y. Yin, Determination of the PCM Melting Temperature Range Using DSC, Thermochimica Acta, 595 (2014), 17-21.
[42] H. Jiang, Y. Tao, J. Jin, Y. Dai, L. Xian, J. Wang, S. Wang, R. Chen, C. Zheng, W. Huang, Resonance-Driven Dynamically Bipolar Organic Semiconductors for High-Performance Optoelectronic Applications, Mater. Horiz. 7 (2020), 3298-3304.
[43] F. Liu, Z. Cheng, L. Wan, L. Gao, Z. Yan, D. Hu, L. Ying, P. Lu, Y. Ma, Anthracene-Based Emitters for Highly Efficient Deep Blue Organic Light-Emitting Diodes with Narrow Emission Spectrum, Chem. Eng. J. 426 (2021), 131351.
[44] S. Chen, Y. Hong, Y. Zeng, Q. Sun, Y. Liu, E. Zhao, G. Bai, J. Qu, J. Hao, B. Z. Tang, Mapping Live Cell Viscosity with an Aggregation-Induced Emission Fluorogen by Means of Two-Photon Fluorescence Lifetime Imaging, Chem. Eur. J. 21 (2015), 4315- 4320.
[45] Y. Xu, X. Liang, Y. Liang, X. Guo, M. Hanif, J. Zhou, X. Zhou, C. Wang, J. Yao, R. Zhao, D.

Hu, X. Qiao, D. Ma, Y. Ma, Efficient Deep-Blue Fluorescent OLEDs with a High Exciton Utilization Efficiency from a Fully Twisted Phenanthroimidazole-Anthracene Emitter, ACS Appl. Mater. Interfaces 11 (2019), 31139-31146.
[46] Y. Xu, X. Liang, X. Zhou, P. Yuan, J. Zhou, C. Wang, B. Li, D. Hu, X. Qiao, X. Jiang, L. Liu, S.-J. Su, D. Ma, Y. Ma, Highly Efficient Blue Fluorescent OLEDs Based on Upper Level Triplet-Singlet Intersystem Crossing, Adv. Mater. 31 (2019), 1807388.
[47] T. Liu, X. Chen, J. Zhao, W. Wei, Z. Mao, W. Wu, S. Jiao, Y. Liu, Z. Yang, Z. Chi, Hybridized Local and Charge-Transfer Excited State Fluorophores Enabling Organic Light-Emitting Diodes with Record High Efficiencies Close to 20%, Chem. Sci. 12 (2021), 5171-5176.